Supplementary Materials:

Lateral Variations of Interplate Coupling along the Mexican Subduction Interface: Relationships with Long Term Morphology and Fault Zone Mechanical Properties

Baptiste Rousset[1], Cécile Lasserre[1], Nadaya Cubas[2], Shannon Graham[3], Mathilde Radiguet[1], Charles DeMets[4], Anne Socquet[1], Michel Campillo[1], Vladimir Kostoglodov[5], Enrique Cabral-Cano[5], Nathalie Cotte[1], Andrea Walpersdorf[1]

---

[1] ISTerre, CNRS, Univ. Grenoble Alpes, F-38041, Grenoble, France

[2] Institut des Sciences de la Terre de Paris, Pierre et Marie Curie University, Paris, France

[3] Department of Earth and Planetary Sciences, Harvard University, Cambridge, Massachusetts, USA

[4] Department of Geoscience, University of Wisconsin-Madison, Madison, Wisconsin, USA

[5] Instituto de Geofisica, Universidad Nacional Autónoma de México, CU, Coyoacan, México

1 Determination of the transition zone

In order to estimate the localisation on the subduction interface of the transition between partially coupled and fully uncoupled areas, we build simple forward models with a partially coupled area that extends from the trench downdip to a distance D and an uncoupled area inland from distance D. The distance D is varied to examine the fit (Figure S1). Cocos-North America plate convergence velocities calculated with the PVEL model (DeMets et al., 2010) and projected onto the convergence direction are used to determine the coupling coefficient on each fault patch. In Figure S1A, vertical rates have been projected onto a profile perpendicular to the trench. The predicted vertical-rate curve, and in particular, the locations where the predicted velocities are zero or maximized, are particularly useful for indicating the down-dip limit of the partially coupled area. Figure S1B illustrates the tradeoffs in the RMS misfit of the elastic model to the 54 GPS site velocities upon varying the distance D and the coupling values. The model that best fits shape of the velocity profile has a transition zone located at $D \simeq$125 km inland from the coast (175 km from the trench) and an average coupling coefficient of 0.6. The scatter in the GPS site velocities relative to the model predictions is caused by along-strike variations in the coupling that are ignored in our model and the simplistic interface geometry assumed for the model. Numerous subsiding stations that are located $\simeq$300 km from the coast are non-tectonic and instead a consequence of surface compaction in the Mexico City sedimentary basin (López-Quiroz et al., 2009).

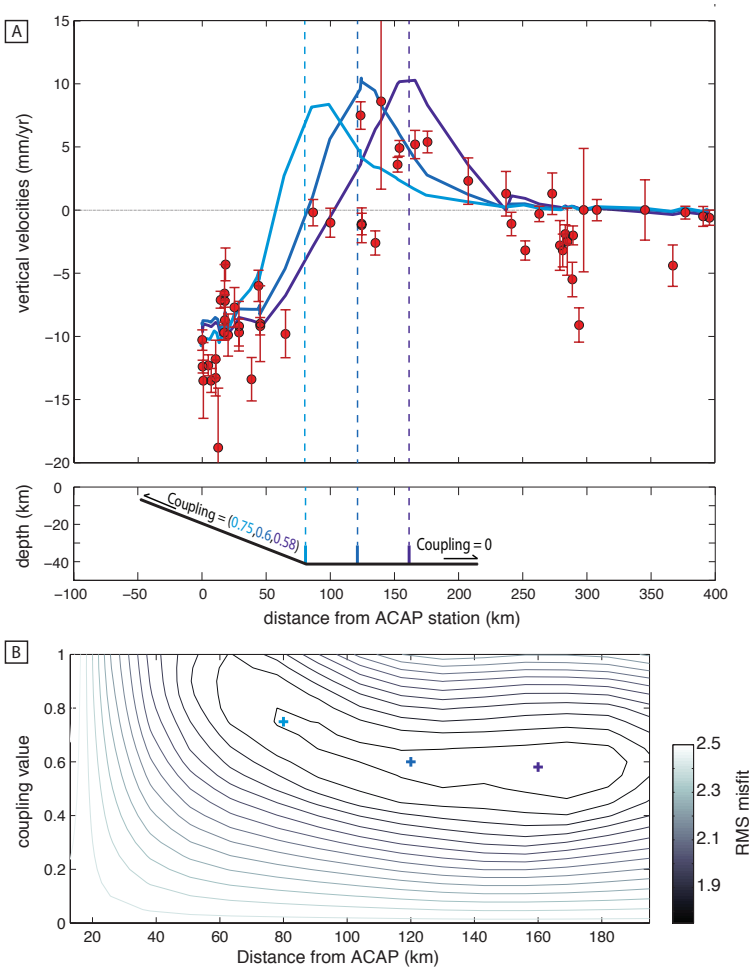

Figure S1: Search for location of the deep transition between uncoupled and coupled areas of the subduction interface. A. Vertical rates measured at GPS stations (red) and predicted by elastic models (blue). The bottom panel shows the geometry and coupling parameters assumed for the three elastic models. Coupling is laterally homogeneous, with values of 0.75 (light blue), 0.6 (blue), and 0.58 (dark blue) variously used for the shallow fault segment and values of zero downdip from D. B. Tradeoffs in RMS misfits as a function of the position of the transition and the coupling assumed for the shallower fault segment. Blue crosses indicate location of the three models presented in A in this space.

2 Coupling inversion method

For a model in which the subduction interface is divided into N patches, the inter-SSE velocity at a given GPS station corresponds to the linear sum of the velocities that are predicted for all N fault patches. The best inter-SSE coupling distribution on the fault patches is found by minimisation of a cost function. Following the approach of Radiguet et al. (2012), we use the least square formulation for linear problems (Tarantola, 2005), where the cost function $S(m)$ is defined as

$$S(m) = \frac{1}{2}\left[(Gm-d)^t C_d^{-1}(Gm-d) + (m-m_0)^t C_m^{-1}(m-m_0)\right] \quad (1)$$

The model solution is given as

$$m = m_0 + C_m G^t \left(GC_m G^t + C_d\right)^{-1}(d - Gm_0) \quad (2)$$

where m_0 is an *a priori* model, G are the Green's functions and C_d and C_m are the data and model covariance matrices, respectively. As mentioned in the main text, for the 2D flat-ramp geometry, the Green's functions are computed following the discrete wave number method (Bouchon, 1981, 2003) in an elastic stratified medium, assuming the Hernandez et al. (2001) velocity model and using AXITRA software (Coutant, 1989). For the Slab1.0 3D geometry, we build the Green's functions using Zhu and Rivera (2002)'s method for the same stratified velocity model. We tested the influence of the prior model on the inversion result using end-member prior models with uniform coupling values of either 1 or 0 (Figure S2). The difference between these two tests is very small and highlights that the solution is mainly constrained by the regularisation, except in areas where coupling values are very poorly resolved, mainly in corners of the designated subduction interface. In our preferred models, we set the prior model to zero. C_d is a diagonal matrix with variances σ^2 related to the standard errors in the GPS site velocity components. As our problem is underdetermined because of the number of observation sites, C_m is a regularisation matrix designed to homogenise the solution by smoothing the coupling pattern, as follows

$$C_m(i,j) = \left(\sigma_m \frac{\lambda_0}{\lambda}\right)^2 e^{-\frac{a(i,j)}{\lambda}} \quad (3)$$

where $a(i,j)$ is the distance between fault patches i and j, σ_m is the standard deviation of the model parameters, λ_0 is a scaling factor equivalent to the patch size, and λ is the correlation length. The function $e^{-\frac{a(i,j)}{\lambda}}$ enables us to stabilise the solution at large distances, whereas coupling on close patches may vary. The sensitivity of the solution to parameters λ and σ_m is presented in Figure S3 for the 2D geometry case, which shows normalised misfits as a function of the model roughness for several values of λ and σ_m. We use the L criterion to select the best couple (λ, σ_m) (Hansen, 1992). Regardless of σ_m, best couples give similar misfits. We select the couple ($\lambda = 80$ $km, \sigma_m = 0.1$ m) which has the most reasonable correlation length compared to the patch size. We use the exact

same parametrisation for the two geometries presented in the paper, in order to see only the effect due to the geometry. The overall coupling pattern is not affected by changing λ. We evaluated the robustness of the solution by computing the model resolution on the interface following Tarantola and Valette (1982), as follows

$$R = C_m G^t (G C_m G^t + C_d)^{-1} G \tag{4}$$

The resolution depends mainly on the sparsity of the GPS network, the number of fault patches and the smoothing applied to achieve the preferred solution. A resolution of 1 corresponds to a fully resolved model, whereas a resolution of 0 means that the model is unpredictable. Diagonal values of the resolution matrix (Figure S5a) specify the resolution of individual fault patches. These are typically low (< 0.3) for the better resolved patches and even lower (< 0.1) for many other patches. The poor resolution per fault patch is a consequence of our relatively fine discretisation of the subduction interface, which we adopted to better localise variations of coupling. Given that smoothing tends to spread the fault coupling over several nearby fault patches, it is important to consider non-diagonal values of the resolution matrix. The sum of rows of the resolution matrix, also called the restitution index, indicates whether the coupling estimated for one fault patch is well reproduced by the sum of the coupling values for nearby, surrounding fault patches. The good density of the Mexican GPS network gives rise to a restitution index of $\simeq 1$ for the entire subduction zone (Figure S5b).

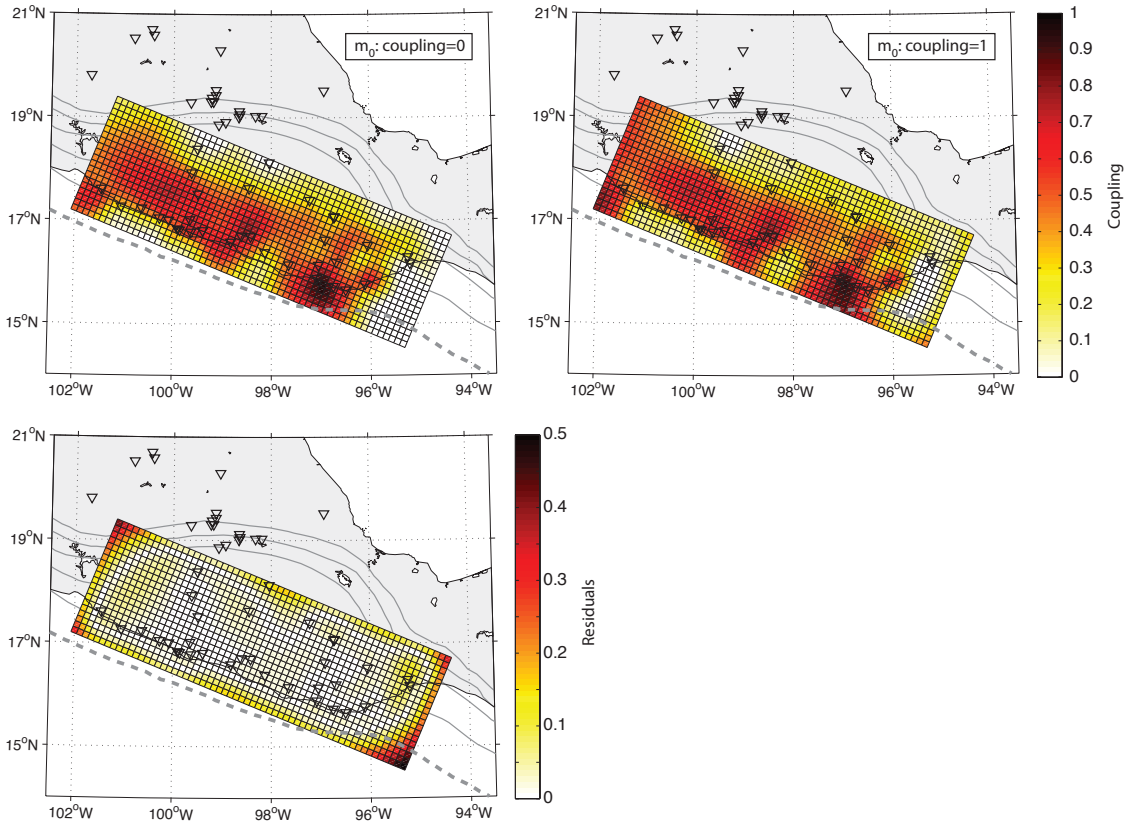

Figure S2: Influence of the *a priori* model m_0 on the inversion solution (example for the 2D flat-ramp slab geometry). The two upper panels present inversion results with homogeneous prior coupling values of 0 and 1 on the whole subduction interface. The bottom panel corresponds to the residuals between the two solutions.

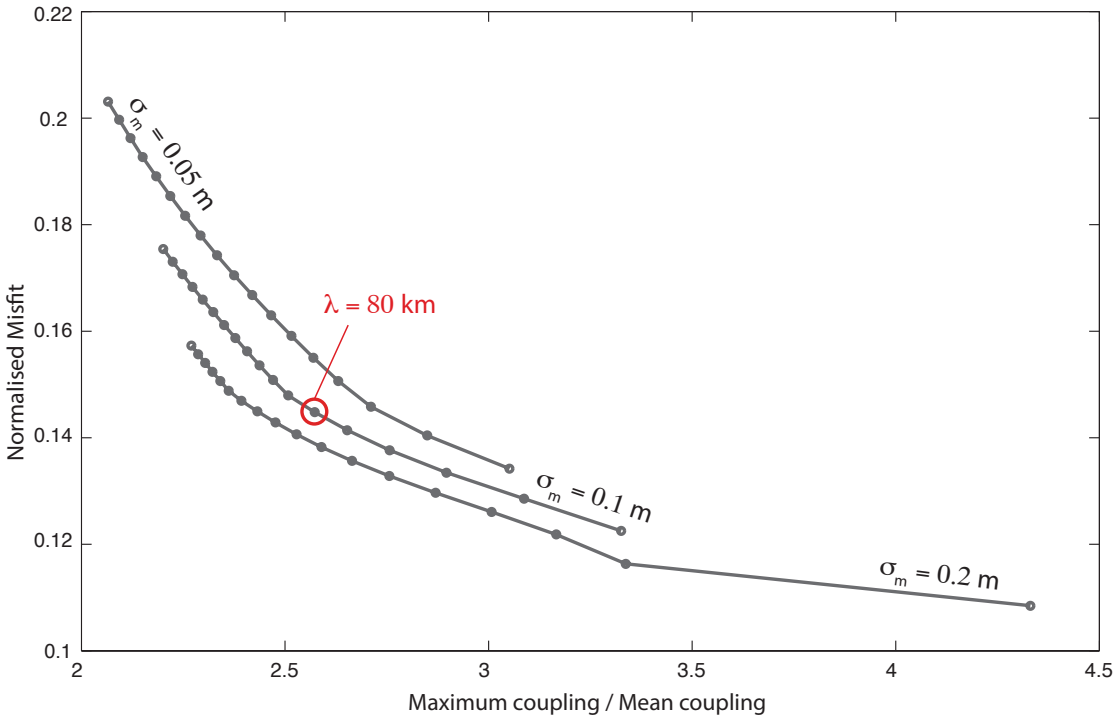

Figure S3: Normalised misfit as a function of the 2D slab geometry model roughness (maximal slip velocity over average slip velocity). Grey points correspond to different λ values from 30 km to 200 km spaced every 10 km. The three curves are relative to σ_m equal to 0.05 m, 0.1 m and 0.2 m. The red circled point, corresponding to the couple (λ = 80 km, σ_m = 0.1 m) is the one used for the preferred inversion.

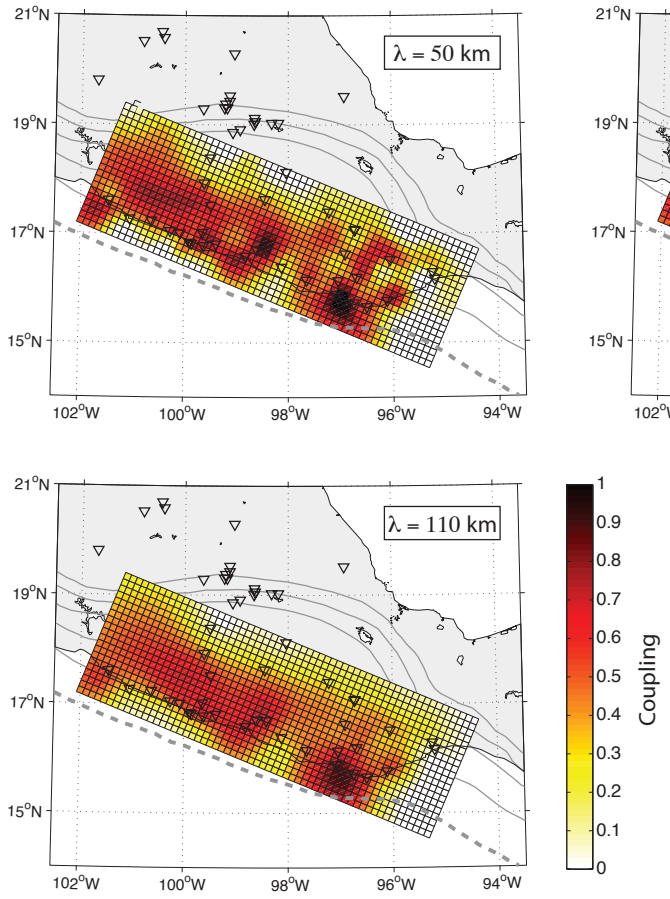

Figure S4: Effect of various smoothing on the inversion (example for the 2D flat-ramp slab geometry). Correlation lengths λ of 50, 80 and 110 km are presented, 80 km being used for the preferred coupling solution.

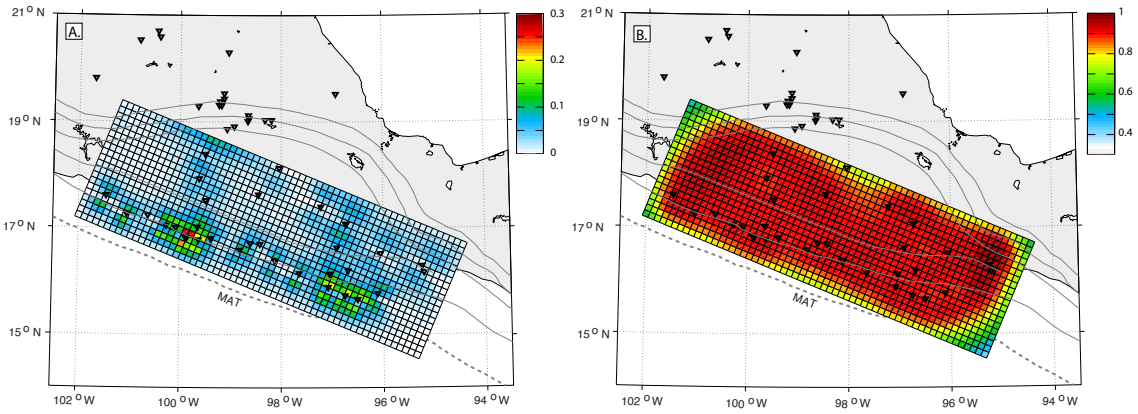

Figure S5: Resolution of the coupling solution (example for the 2D flat-ramp slab geometry). A. Diagonal values of the resolution matrix. B. Restitution index, corresponding to the sum of the rows of the resolution matrix. GPS station locations are indicated by inverse black triangles.

References

Bouchon, M. (1981). A simple method to calculate green's functions for elastic layered media. *Bulletin of the Seismological Society of America*, 71(4):959–971.

Bouchon, M. (2003). A review of the discrete wavenumber method. *Pure and applied Geophysics*, 160(3-4):445–465.

Coutant, O. (1989). Programme de simulation numerique axitra. *Rapport LGIT*.

DeMets, C., Gordon, R. G., and Argus, D. F. (2010). Geologically current plate motions. *Geophysical Journal International*, 181(1):1–80.

Hansen, P. C. (1992). Analysis of discrete ill-posed problems by means of the l-curve. *SIAM review*, 34(4):561–580.

Hernandez, B., Shapiro, N., Singh, S., Pacheco, J., Cotton, F., Campillo, M., Iglesias, A., Cruz, V., Gómez, J., and Alcántara, L. (2001). Rupture history of september 30, 1999 intraplate earthquake of oaxaca, mexico (mw= 7.5) from inversion of strong-motion data. *Geophysical research letters*, 28(2):363–366.

López-Quiroz, P., Doin, M.-P., Tupin, F., Briole, P., and Nicolas, J.-M. (2009). Time series analysis of mexico city subsidence constrained by radar interferometry. *Journal of Applied Geophysics*, 69(1):1–15.

Radiguet, M., Cotton, F., Vergnolle, M., Campillo, M., Walpersdorf, A., Cotte, N., and Kostoglodov, V. (2012). Slow slip events and strain accumulation in the guerrero gap, mexico. *Journal of Geophysical Research: Solid Earth (1978–2012)*, 117(B4).

Tarantola, A. (2005). *Inverse problem theory and methods for model parameter estimation*. Society for Industrial & Applied.

Tarantola, A. and Valette, B. (1982). Generalized nonlinear inverse problems solved using the least squares criterion. *Reviews of Geophysics*, 20(2):219–232.

Zhu, L. and Rivera, L. A. (2002). A note on the dynamic and static displacements from a point source in multilayered media. *Geophysical Journal International*, 148(3):619–627.